Study of $X(3872)$ and $X(3915)$ using Belle detector

Ashish Thampi

MS12118

A dissertation submitted for the partial fulfilment of

BS-MS dual degree in Science

Indian Institute of Science Education and Research Mohali

April 2017

Certificate of Examination

This is to certify that the dissertation titled **"Study of $X(3872)$ and $X(3915)$ using Belle detector"** submitted by **Mr. Ashish Thampi** (Reg. No. MS12118) for the partial fulfilment of BS-MS dual degree programme of the Institute, has been examined by the thesis committee duly appointed by the Institute. The committee finds the work done by the candidate satisfactory and recommends that the report be accepted.

Dr. Vishal Bhardwaj (Supervisor) Dr. Smriti Mahajan Dr. Ketan Patel

Dated: April 21, 2017

Declaration

The work presented in this dissertation has been carried out by me under the guidance of Dr. Vishal Bhardwaj at the Indian Institute of Science Education and Research Mohali.

This work has not been submitted in part or in full for a degree, a diploma, or a fellowship to any other university or institute. Whenever contributions of others are involved, every effort is made to indicate this clearly, with due acknowledgement of collaborative research and discussions. This thesis is a bonafide record of original work done by me and all sources listed within have been detailed in the bibliography.

Ashish Thampi

(Candidate)

Dated: April 21, 2017

In my capacity as the supervisor of the candidate's project work, I certify that the above statements by the candidate are true to the best of my knowledge.

Dr. Vishal Bhardwaj

(Supervisor)

Acknowledgement

I express my gratitude to all those who helped me, in making this project a pleasant experience. I would like to extend my sincere thanks to all of them.

I am highly indebted to Dr. Vishal Bhardwaj for his guidance and constant supervision. I am really obliged to him for giving me this opportunity.

I sincerely thank Dr. Ketan Patel and Dr. Smriti Mahajan for the fruitful discussions which helped me to understand the subject better.

I would like to express my gratitude towards my parents and friends for their support and encouragement which helped me in the completion of this project.

I thank Belle Collaboration for providing necessary computation power and resources utilised in this project.

I acknowledge IISER Mohali for providing best facilities and environment for carrying out the project. I also thank Department of Science and Technology, Govt. of India for supporting me with INSPIRE fellowship during the past five years.

List of Figures

Contents

Abstract

Last decade has seen the discovery of many exotic charmonium-like states. $X(3872)$ is the poster boy of such exotic states. The nature of $X(3872)$ is still unknown. Precise measurement of $R_{3\pi/2\pi} = \frac{\mathcal{B}(X(3872)\to J/\psi\pi^+\pi^-\pi^0)}{\mathcal{B}(X(3872)\to J/\psi\pi^+\pi^-)}$ is crucial to understand the nature of $X(3872)$ state. We performed Monte Carlo study for $B^\pm \to (J/\psi\omega)K^\pm$ decay at Belle detector. We estimated the reconstruction efficiency for $B^\pm \to X(3872)K^\pm$ and $B^\pm \to X(3915)K^\pm$ decay modes. Based on that we expect 35 (170) signal events for $X(3872) \to J/\psi\omega$ ($X(3915) \to J/\psi\omega$) from the $\Upsilon(4S)$ data collected by Belle detector at KEKB asymmetric electron-positron collider.

Chapter 1

Introduction

1.1 Mesons

Hadrons which are composed of one quark and one antiquark, are known as "Mesons". They are bosons by nature, as they have an integral spin (0,1). Since mesons are composed of quarks, they participate in both weak and strong interactions. Mesons with electric charge participate in electromagnetic interactions. The quark has an intrinsic angular momentum termed as spin, which takes values $S = \pm 1/2$. Two quarks add up their spin vectors and result in $S = 0,\ 1$. There will be $2S + 1$ spin projections. Thus spin-1 triplet and spin-0 singlet exist. That is mesons can be found in triplet and singlet spin states.

Due to the quarks orbiting each other, another quantized quantity exists, orbital angular momentum, L. The total angular momentum of a particle (J) can be any values in between $|L - S|$ and $|L + S|$ in increment of 1.

1.2 Charmonium

Charmonium is composed of charm quark (c) and antiquark ($\bar{c}$). Charmonium family have a net charm zero. In simple assumption, they are subjected to a central potential known as Cornell potential:

$$V(r) = -\frac{4}{3}\frac{\alpha_s}{r} + kr \tag{1.1}$$

where first term represents the asymptotic freedom (single gluon exchange) and second term the confinement. Distance between quarks is denoted as r. α_s and k are

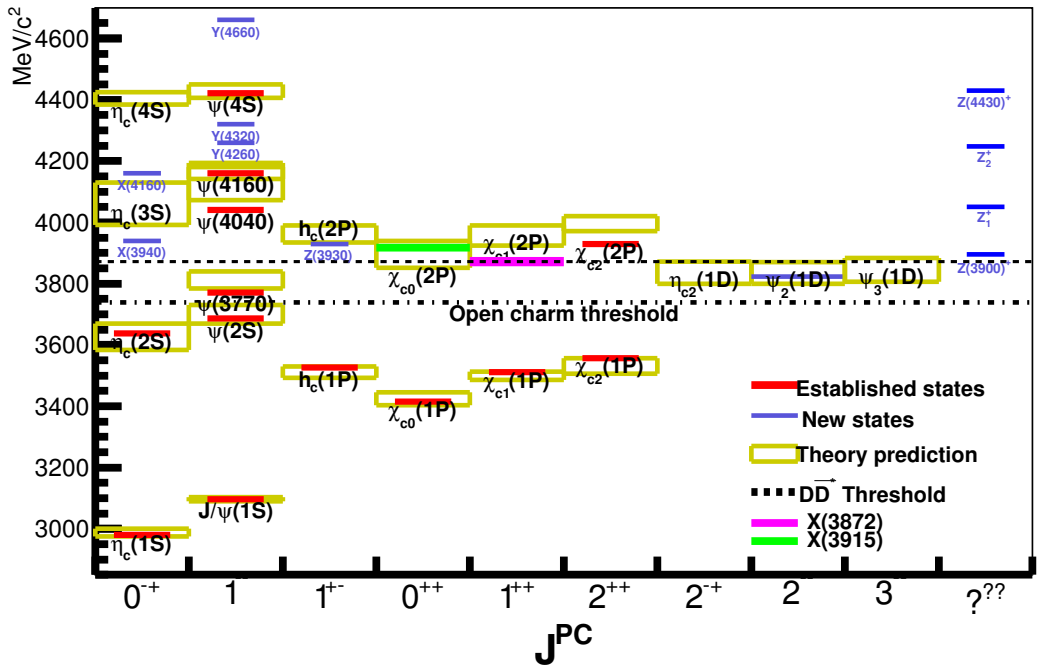

Figure 1.1: Charmonium spectrum comparing theory and experimental results

determined from the fit to data. Using this potential, charmonium spectra is reproduced. This non-relativistic treatment describes the feature of charmonium levels. Including the spin dependent interactions, resolve the degeneracy among spin multiplets.

As a minimal model of charmonium system, one can use the standard color Coulomb plus linear scalar form and also include a Gaussian-smeared contact hyperfine interaction. The non-relativistic potential will become [1],

$$V_0(r) = -\frac{4}{3}\frac{\alpha_s}{r} + kr + \frac{32\pi\alpha_s}{9m_c^2}\delta_\sigma(r)\vec{S}_c \cdot \vec{S}_{\bar{c}} \tag{1.2}$$

where $\delta_\sigma(r) = (\sigma/\sqrt{\pi})^3 e^{-\sigma^2 r^2}$. These parameters are obtained from fitting the spectrum. From experimental output, one can use the masses of 11 reasonably well established $c\bar{c}$ states, and obtain the above said parameters by fitting these masses. From these values masses of currently unknown $c\bar{c}$ states can be predicted.

Comparison between experimentally observed spectrum and the predictions of conventional $c\bar{c}$ model is shown in Figure 1.1. Below the open charm threshold of $D\bar{D}$, the agreement between the experiment and theory is remarkable. However, above and

near the $D\bar{D}$ threshold, one can see a discrepancy between predicted and observed states. Further, many new states have been found which suggest that our understanding of charmonium states (along with exotic states) is very limited. Input from theory and experiment is needed to improve our understanding.

1.3 Charmonium production

In B-factories charmonium can be produced by four processes:

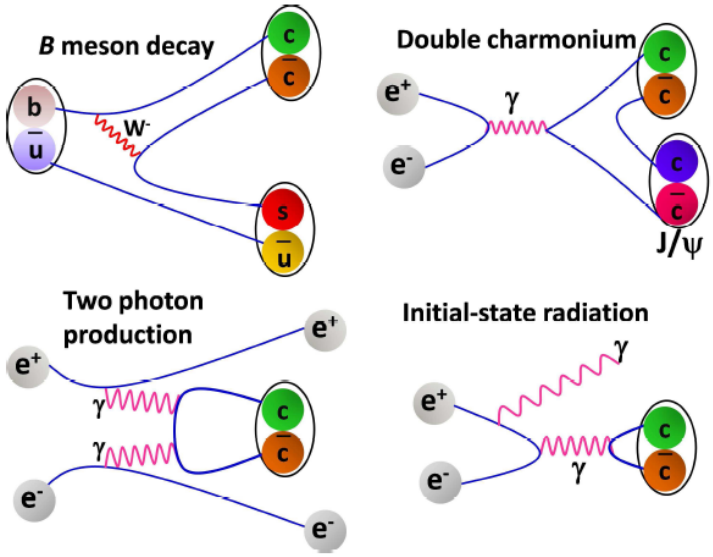

Figure 1.2: The processes leading to the production of charmonium at the B factories.

- B meson decay

  Through this decay charmonium states along with K mesons are produced with a good fraction. Large $\Upsilon(4S)$ data available at B factories provide unique opportunity to study known states or find new resonances. Charmonium with any quantum number can be produced in two body decays of B mesons.

- Two photon production

  Electron-positron annihilation at higher energies produce charmonium states (0^{-+}, 0^{++}, 2^{-+}, 2^{++}) through two virtual photons via the process

$$e^+e^- \rightarrow e^+e^- + (c\bar{c}) \tag{1.3}$$

Both e^+ and e^- radiate photons that subsequently interact with each other. These type of charmonium states have positive C-parity.

- Initial state radiation

  In this process, either electron or positron radiates a photon before annihilation, which results in lowering the effective CM energy. Only $J^{PC} = 1^{--}$ states can be produced in ISR.

- Double charmonium

  The production of double charmonium states in e^+e^- annihilation was discovered by Belle collaboration. Despite the small cross-section value these studies are possible because of high luminosity B factories. In the process of pair charmonium production in e^+e^- annihilation, the final charmonium states have opposite charge parities.

1.4 Exotic charmonium-like states

Recently, states have been discovered which can not be easily accommodated in the conventional mesons and baryons model. As these states do not fit the conventional state properties, they are called exotic states. A decade earlier only a handful of exotic states were known. But with the advent of high statistics collider experiments, many exotic states are known and are well established.

1.4.1 Search for exotic charmonium-like states

For the search of non-conventional charmonium, decay modes with enhanced production of new resonant states are studied. The invariant mass distribution of $J/\psi\omega$ is known for the search of $X(3872)$ and $X(3915)$. $J/\psi\omega$ invariant mass system is analysed in B decays ($B \to J/\psi\omega K$) [2].

1.4.2 $X(3872)$

$X(3872)$ was first seen in 2003 by the Belle Collaboration at KEKB, Japan as a narrow peak in the $J/\psi\pi^+\pi^-$ invariant mass distribution at 3872 MeV/c^2 in the decay $B \to J/\psi\pi^+\pi^-K$ [3]. The letter X was chosen because of its unknown properties and

the observed $J/\psi\pi^+\pi^-$ decay mode was not assigned to any known charmonium. BaBar had observed $X(3872)$ and $X(3915)$ in $J/\psi\omega$ invariant mass distribution in the $B \to J/\psi\omega(\to \pi^+\pi^-\pi^0)K$ decay mode [4].

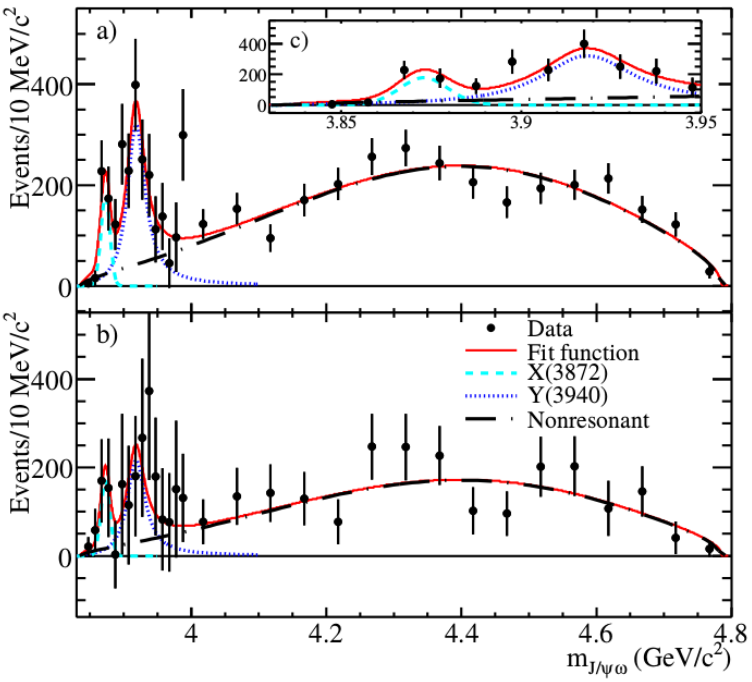

Figure 1.3: The $M_{J/\psi\omega}$ distribution for (a) B^+, (b) B^0 decays; (c) shows the low mass region of (a) in detail. $X(3915)$ was previously known as $Y(3940)$. [4]

Theoretical models for $X(3872)$

In an attempt to explain the properties of $X(3872)$, many models were predicted [5]. Out of which, some of the few famous models are

- Excited charmonium state

  The observed decay in J/ψ implies that $X(3872)$ must contain a $c\bar{c}$ pair. However, branching fraction for $X(3872)$ decay to $D\bar{D}^*$ is larger than its decay to $J/\psi\pi^+\pi^-$, which is not easy to explain in case of pure charmonium.

- Mesonic molecule

  $X(3872)$ mass is very close to the sum of the masses of the D^0 and $\bar{D}^{*0}$ mesons. The difference between the observed mass and threshold is regarded as the binding energy and it is small. It speculated that $X(3872)$ could be a $D^0 - \bar{D}^{*0}$

loosely bound state. Then $X(3872)$ must be so fragile and its production at "hadron colliders" (such as CDF, LHC and DO) is puzzling [6].

- Tetraquark

  In tetraquark hypothesis for $X(3872)$, a mass splitting due to mixing between $c\bar{c}u\bar{u}$ and $c\bar{c}d\bar{d}$ is theoretically predicted. The mass difference is expected to appear as the difference in masses of X separately measured in $B^{\pm} \to XK^{\pm}$ and $B^0 \to XK^0$. The experimental result[7] for this value strongly disfavours the tetraquark interpretation.

- Admixture of molecular state and charmonium

  In the admixture scenario, the $X(3872)$ is comprised of mainly the $\bar{D}^0 \bar{D}^{*0}$ molecule and also contain sizable $\chi_{c1}(2P)$ component.

2π and 3π decays

$X(3872)$ was discovered in the $J/\psi\pi^+\pi^-$ channel and then its $J/\psi\pi^+\pi^-\pi^0$ decay was observed. According to the experiments the $\pi^+\pi^-$ state in the $X(3872) \to J/\psi\pi^+\pi^-$ decay arises from the ρ meson having isospin = 1. Since no signal of charged partners has been observed $X(3872)$ is considered to be an iso-singlet state. That means the $\pi^+\pi^-$ decay of $X(3872)$ is iso-spin violating. So the ratio of branching fractions $R_{3\pi/2\pi}$ is interesting to be studied.

$$R_{3\pi/2\pi} = \frac{\mathcal{B}(X(3872) \to J/\psi\pi^+\pi^-\pi^0)}{\mathcal{B}(X(3872) \to J/\psi\pi^+\pi^-)} \tag{1.4}$$

Using BaBar measured $\mathcal{B}(X(3872) \to J/\psi\pi^+\pi^-\pi^0)$, one can get $R_{3\pi/2\pi} = 0.8 \pm 0.3$ [4]. The Belle have more data accumulated and more precise value for this ratio can be calculated. This ratio is a crucial input for understanding the nature of $X(3872)$[9].

Chapter 2

Experimental setup

2.1 KEKB collider

The KEKB is an asymmetric energy e^-e^+ collider with e^- having energy 8 GeV and e^+ having energy 3.5 GeV. The centre of mass energy ($\sqrt{s}$) is equal to the mass of $\Upsilon(4S)$ resonance. The $\Upsilon(4S)$ is a bound state of $b\bar{b}$ and having mass just above the threshold $B\bar{B}$ production [10].

$$\sqrt{s} = \sqrt{4E_{e^+}E_{e^-}} = 10.58\text{GeV} \tag{2.1}$$

The $\Upsilon(4S)$ mainly decays to $B^0\bar{B}^0$ or B^+B^- in equal amount. B is the bound state of $\bar{b}u$ or $\bar{b}d$ quarks.

$$\frac{\Gamma(\Upsilon(4S) \to B^+B^-)}{\Gamma(\Upsilon(4S) \to B^0\bar{B}^0)} = 1.065 \pm 0.026 \tag{2.2}$$

Large number of B mesons are necessary for the studies because of the very small branching fractions of B decays (typical $\mathcal{O}$ of 10^{-6}). The KEKB machine is designed to provide about 10^8 B mesons per year.

2.2 KEKB accelerator

The accelerator[11] consists of two rings in which the beam is sent through linear accelerator. The electron beam and positron beam are injected into the rings: the high energy ring (HER) contains electrons at 8.0 GeV and low energy ring (LER)

contains positrons at 3.5 GeV. These beams collide at the interaction point (IP), where they cross each other in the centre of Belle detector. To reduce the beam-beam interaction away from IP, beams are made to intersect at a finite angle (22 mrad); which removes the need of separation magnets inside the detector volume. This raises the effective beam cross-sectional area, which results in the reduction of specific luminosity of collisions.

2.3 Belle detector

The Belle detector[12] is constructed to carry out quantitative study of B meson decays especially the rare B decay modes with very small branching fractions. B mesons are very short-lived particles and it decay instantaneously into relatively long life time particles before they reach the innermost part of the detector. Belle detector detects the particles namely $e^{\pm}$, $\mu^{\pm}$, $\pi^{\pm}$, $K^{\pm}$, p, $\bar{p}$, γ and K^0. The neutron and anti-neutron which are produced cannot be detected.
Belle consist of concentric layers of sub-detectors designed to provide momentum and position information via magnetic spectroscopy, energy measurements via electromagnetic calorimeter, and particle identification through energy loss and penetration depth data. The sub-detectors are:

- Silicon vertex detector (SVD)
- Central drift chamber (CDC)
- Aerogel cerenkov counter (ACC)
- Time of flight scintillator (TOF)
- Electromagnetic calorimeter (ECL)
- Kaon and muon detector (KLM)
- Extreme forward calorimeter (EFC)

Beam pipe is the inner-most part of the detector and all the particles pass through it before reaching SVD. Double walled Beryllium cylinder is used as beam-pipe for two

reasons. It should be such thick as to withstand the beam induced heating and the material should be minimum to avoid Coulomb scattering. The SVD provides precise measurement of the decay vertices of B mesons. SVD2 consists of four cylindrical layers whose radii are 20.0 mm, 43.5 mm, 70.0 mm and 88.0 mm. The angular acceptance is 17^0 to 150^0. The CDC determines the three dimensional trajectories and momenta of charged particles. A superconducting solenoid provides a 1.5 T magnetic field and it bends the charged particle according to their momenta. In addition, CDC measures the energy loss (dE/dx) of charged particles. Identification of $\pi^{\pm}$ and $K^{\pm}$ is very important. In the momentum region below 1 GeV/c, dE/dx measurement from CDC and the time of flight measurements are used to perform K/π separations. The ACC provides the K/π separation in momentum range of $1.2 < p < 3.5$ GeV/c by detection of the cherenkov light from particle penetrating through silica aerogel radiator. Time of flight detector system has a time resolution of 100 ps. The counters measure the elapsed time between collision at IP and hitting of particle at TOF layers. From this measured time from TOF and measured flight length and momentum from CDC, one can estimate the mass of each track in the event.

Figure 2.1: Belle detector and order of sub-detectors

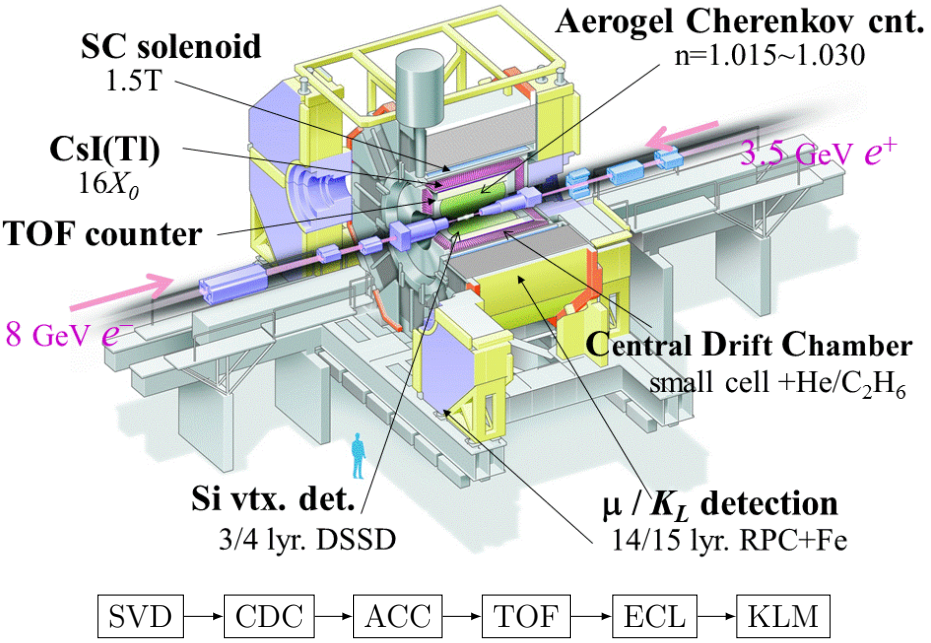

An electromagnetic cascade as pair production and Bremsstrahlung is initiated when a high energy electron or photon is incident on a thick observer, which generate more electrons and photons with lower energy. ECL detects photons with high

efficiency and good resolutions in energy and position. Most of the photons are end products of the cascade decays. So ECL should have a good performance below 500 MeV. High energy photons (up to 4 GeV) are also produced from some decay modes and high resolution is needed to reduce the background for these modes. The electron is identified using the following informations.

- Matching the charged track measured by the CDC and that of the energy cluster measured by ECL.
- Ratio of energy measured by ECL to momentum measured by CDC, E/p.
- dE/dx in CDC.
- Light yield in ACC.

A charged particle with momentum vector at an angle with respect to the magnetic field, will have a helical trajectory. The momentum magnitude can be determined from the radius of curvature of helix. To measure the particle momentum in CDC , 1.5 T magnetic field is applied parallel to the beam-pipe. The K_L^0/μ (KLM) detector detect K_L^0 mesons and identify muons. It is the only detector which is outside the solenoid magnetic field. K_L^0 particles live long so that it will travel beyond ECL. They induce showers of ionizing particles in ECL and it continue into KLM. The position information of K_L^0 is provided by the detector. Muons lose their energy mostly through ionization process. They penetrate ECL easily and continue through most of all KLM. KLM tracks matching with CDC tracks are identified as muons.

Table 2.1: How particle is identified

Particle	Energy	Momentum	Position	Particle identification
$e^-(e^+)$	ECL	CDC	SVD,CDC	ECL,ACC,TOF,CDC
$\mu^-(\mu^+)$		CDC	SVD,CDC	KLM,ACC,TOF,CDC
$\pi^-(\pi+)$		CDC	SVD,CDC	ACC,TOF,CDC
$K^-(K^-)$		CDC	SVD,CDC	ACC,TOF,CDC
$p(\bar{p})$		CDC	SVD,CDC	ACC,TOF,CDC
γ	ECL		ECL	ECL,CDC
K_L			KLM	KLM

Chapter 3

Analysis

3.1 Blind analysis

To minimize the possibility of bias in experimental results, blind analysis strategies are used. The measurement depends upon the cuts we are using to get the result. So the experimenter will not look at the result before optimizing all the cuts. Otherwise one can tune their cuts on data to get the needed significance. Analysis carried out here is performed by blinding the signal region in data.

3.2 Signal Monte Carlo

One million signal events are simulated using EvtGen and GSim. The simulated decay scheme is shown in Figure 3.1.

3.2.1 Event generation

The monte carlo (MC) signal events are generated using EvtGen[13] as an event generator and the response of the Belle detector is simulated using GEANT3-based CERN program[14]. EvtGen is an event generator designed for the simulation of the physics of B decays. It makes B decay products according to the decay defined by the user. If user's specific decay table is not specified then events will be generated according to generic decay table. Geant is the repository of all particle interactions. Thus the full detector simulation is performed using the Geant package.

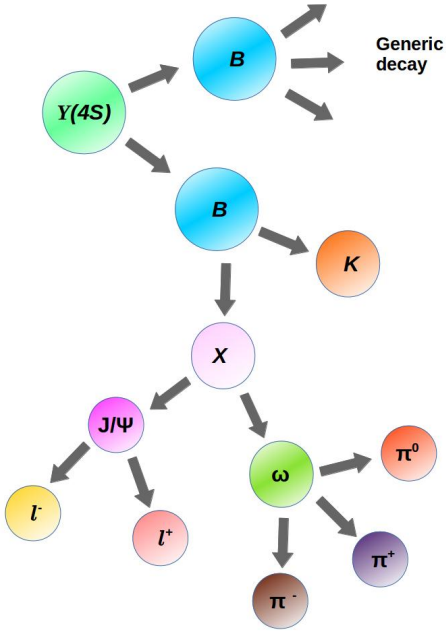

Figure 3.1: The decay scheme

3.2.2 Analysing the generated events

An analysis code is written in C++ to study the MC events.

Figure 3.2: Flow chart for the analysis code

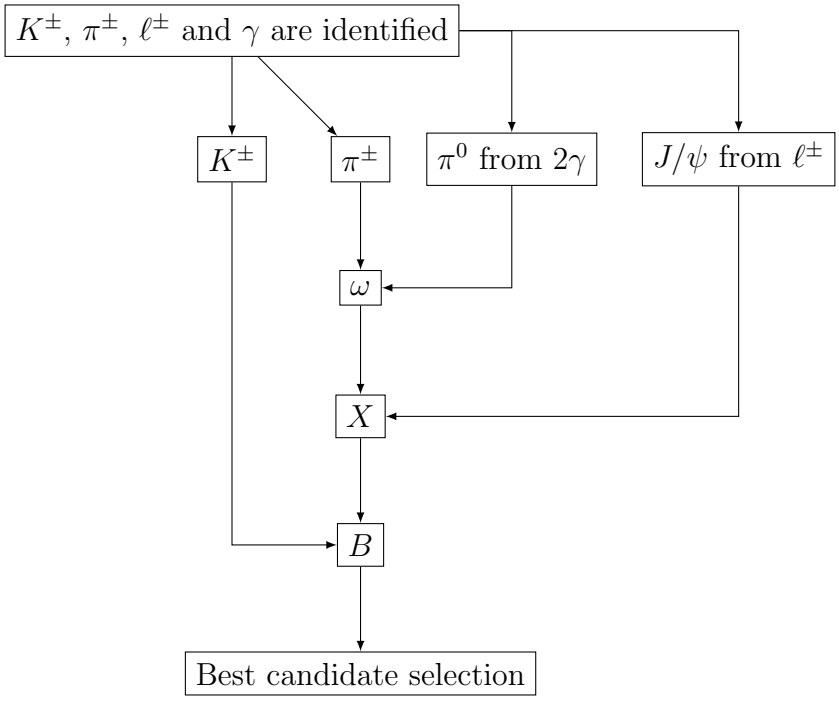

3.3 Particle identification

B meson is reconstructed from the decay particles. The particles used to reconstruct B meson are $e^{\pm}$, $\mu^{\pm}$, $K^{\pm}$, $\pi^{\pm}$, γ. These are the final particles which are detected by the detector for our decay.

Basic cuts and criterions

- To suppress the background coming from the continuum events ($e^+e^- \rightarrow q\bar{q}$), ratio of second to zeroth Fox-Wolfram moments is used[15].

$$R_2 = \frac{H_2}{H_0} \tag{3.1}$$

$$H_k = \sum_{i,j} |p_i||p_j| P_k(cos\theta_{ij}) \tag{3.2}$$

  Here p_i is the four momentum of i-th track and $cos\theta_{ij}$ is the angle between i-th and j-th tracks. P_k is the Legendre polynomial. R_2 will be 0 for a perfect spherical event. The $B\bar{B}$ mesons are produced almost at rest and their decay axis are uncorrelated, which means these events are almost spherical in shape. So it can be distinguished from the jet like continuum events of u,d,s or c. In attempt to reduce this continuum background, R_2 parameter is chosen to be less than 0.5.

- Distance in the $x-y$ plane from the interaction point to the particle, dr
  -1.0 cm $<$ dr $<$ 1.0 cm

- Distance in the z axis from the interaction point to the particle, dz
  -3.5 cm $<$ dz $<$ 3.5 cm

3.3.1 π/K selection

The pion or kaon is identified based on the likelihood ratio calculated from the sub-detector measurements.

$$\mathcal{R}(\pi(\mathcal{K})) = \frac{\mathcal{L}_{\pi(\mathcal{K})}}{\mathcal{L}_{\pi} + \mathcal{L}_{\mathcal{K}}} \tag{3.3}$$

$$\mathcal{R}(\pi) = 1 - \mathcal{R}(\mathcal{K}) \tag{3.4}$$

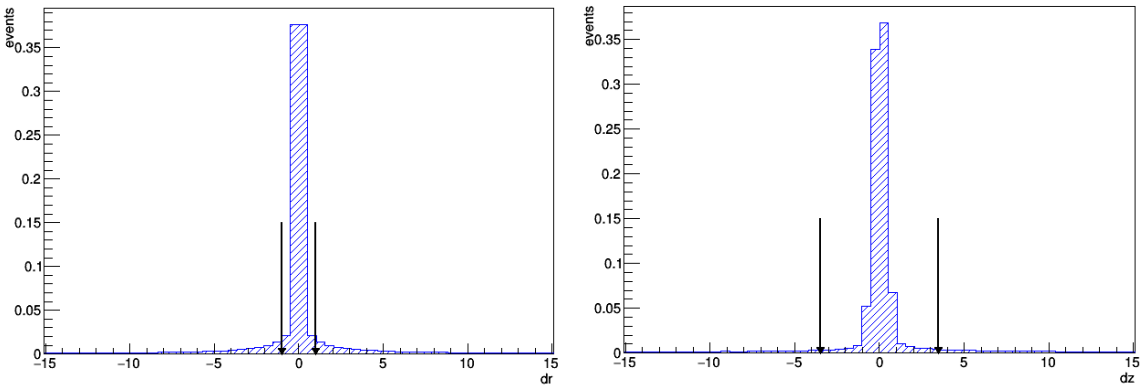

Figure 3.3: dr and dz plots

In our analysis kaon candidates are identified by the cut made on kaon likelihood ratio, $\mathcal{R}(\mathcal{K}) > 0.6$ and charged pions are identified with $\mathcal{R}(\pi) > 0.6$.

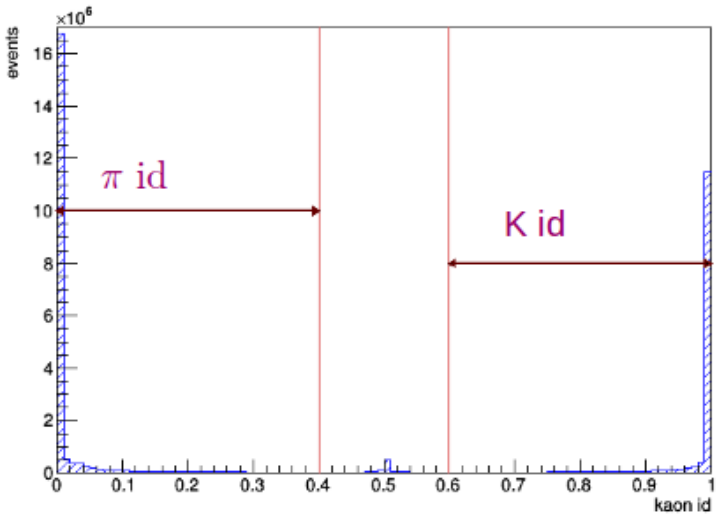

Figure 3.4: $R(K)$ distribution

3.3.2 μ, e identification

Using the information of track penetration depth from KLM system muons are identified. Electrons are identified using the E/p ratio (energy, E from ECL and momentum, p from CDC and SVD) and dE/dx from CDC.

3.3.3 γ selection

In Belle detector, γ candidate is based upon their EM interactions inside the ECL (a shower production mechanism). Selection criteria applied on the EM shower is

$E_9/E_{25} > 0.85$, where $E_9(E_{25})$ is the energy deposited in the $3 \times 3(5 \times 5)$ crystals in the ECL.

3.4 Reconstruction

Using the identified final states, intermediate and primary states can be reconstructed.

3.4.1 π^0 reconstruction

Neutral pions are reconstructed by combining two photons with energy greater than 60 Mev. In MC when the mass of π^0 is compared, it became clear that $\pm 2\sigma$ cut can be applied to select the π^0 more efficiently. In figure 3.5, it can be seen that the signal efficiency can be increased by applying a 2σ cut. Thus we can remove more fake π^0 candidates. The π^0 candidates are identified as 123 MeV/c^2 $< M_{\pi^0} <$ 147 MeV/c^2.

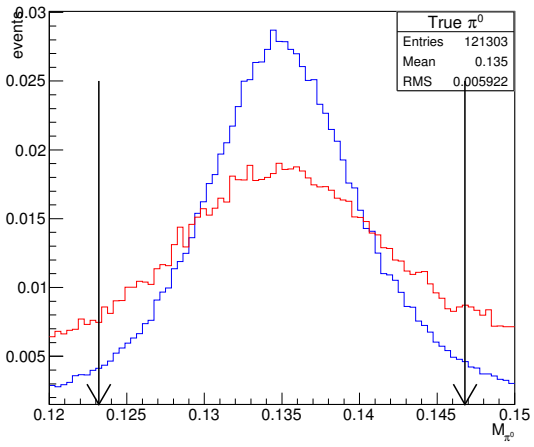

Figure 3.5: M_{π^0} plot. The blue one is the true π^0 and red one represents the fake π^0. The cut used is 123 MeV/c^2 $< M_{\pi^0} <$ 147 MeV/c^2

3.4.2 ω from pions

ω is reconstructed by combining the particles π^+, π^-, π^0. Among the reconstructed candidates ω is identified as 0.700 GeV/c^2 $< M_\omega <$ 0.850 GeV/c^2.

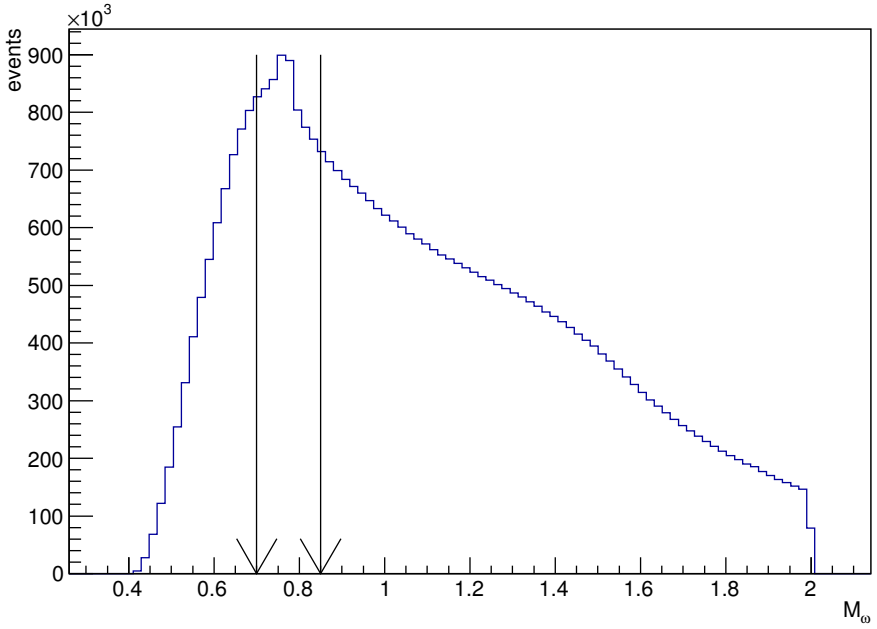

Figure 3.6: ω reconstruction

3.4.3 Reconstruction of J/ψ

J/ψ is reconstructed using $\ell^+\ell^-$, where ℓ is electron or muon. Different cuts are used to select the J/ψ candidates for e and μ. The cut corresponding to $\mu^+\mu^-$ is 3.07 GeV/c^2 $< M_{\mu\mu} <$ 3.13 GeV/c^2. There is a loss of energy from electron in the form of emission of bremsstrahlung photons. The four momenta of the photons within 0.05 radian of e^+ or e^- direction are included in the invariant mass calculation. However, even after this correction, the $J/\psi \to e^+e^-$ signal shape is still skewed, which is taken into account by using an asymmetric invariant mass window 3.05 GeV/c^2 $< M_{ee\gamma}$ 3.13 GeV/c^2 to define the J/ψ candidate in the electron channel. Also, J/ψ candidates are selected with momentum less than 2 GeV/c^2 to avoid direct J/ψ coming from B meson decay.

3.4.4 Reconstruction of $X(3872)$ and $X(3915)$

$X(3872)$ and $X(3915)$ are reconstructed by combining J/ψ and ω. Hereafter, X refers either to $X(3872)$ or $X(3915)$, unless explicitly mentioned.

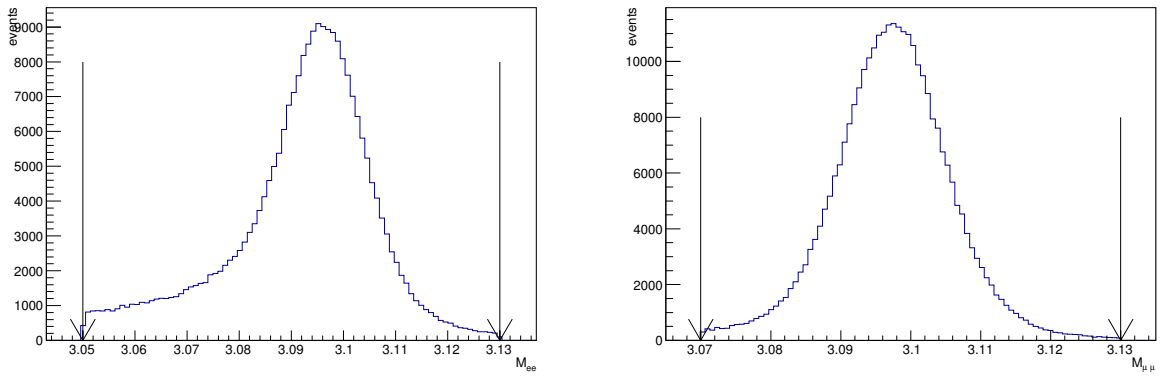

Figure 3.7: J/ψ reconstruction from $e^+e^-\gamma$ (left) and $\mu^+\mu^-$ (right)

3.4.5 B reconstruction

The reconstruction of B meson is done by combining the reconstructed daughters. According to the decay, B is reconstructed by combining X and $K^{\pm}$.

$$B \to X + K^{\pm} \tag{3.5}$$

Some variables are defined to identify B meson. Beam constrained mass, $M_{\rm bc}$ and ΔE.

$$M_{\rm bc} = \sqrt{E^2_{beam} - (p_X + p_{K^{\pm}})^2} \tag{3.6}$$

$$\Delta E \equiv (E_X + E_{K^{\pm}}) - E_{beam} \tag{3.7}$$

E_{beam} is the beam energy in centre of mass (CM) frame and $p_{X(K^{\pm})}$, $E_{X(K^{\pm})}$ are the momentum and energy of the $X(K^{\pm})$ candidate in the CM frame of $\Upsilon(4S)$. In ideal case ΔE should be zero and $M_{\rm bc}$ will peak around the nominal B mass (which is 5.279 GeV/c^2).

The grand selection for B meson candidates was taken as -0.2 GeV $<$ ΔE $<$ 0.2 GeV and $M_{\rm bc}$ $>$ 5.20 GeV/c^2 region. Signal window for $M_{\rm bc}$ is defined as $M_{\rm bc}$ $>$ 5.27 GeV/c^2.

ΔE figure of merit

The reconstructed event can be signal or background. In order to remove the background with less signal loss we define a small selection window for the ΔE, so that

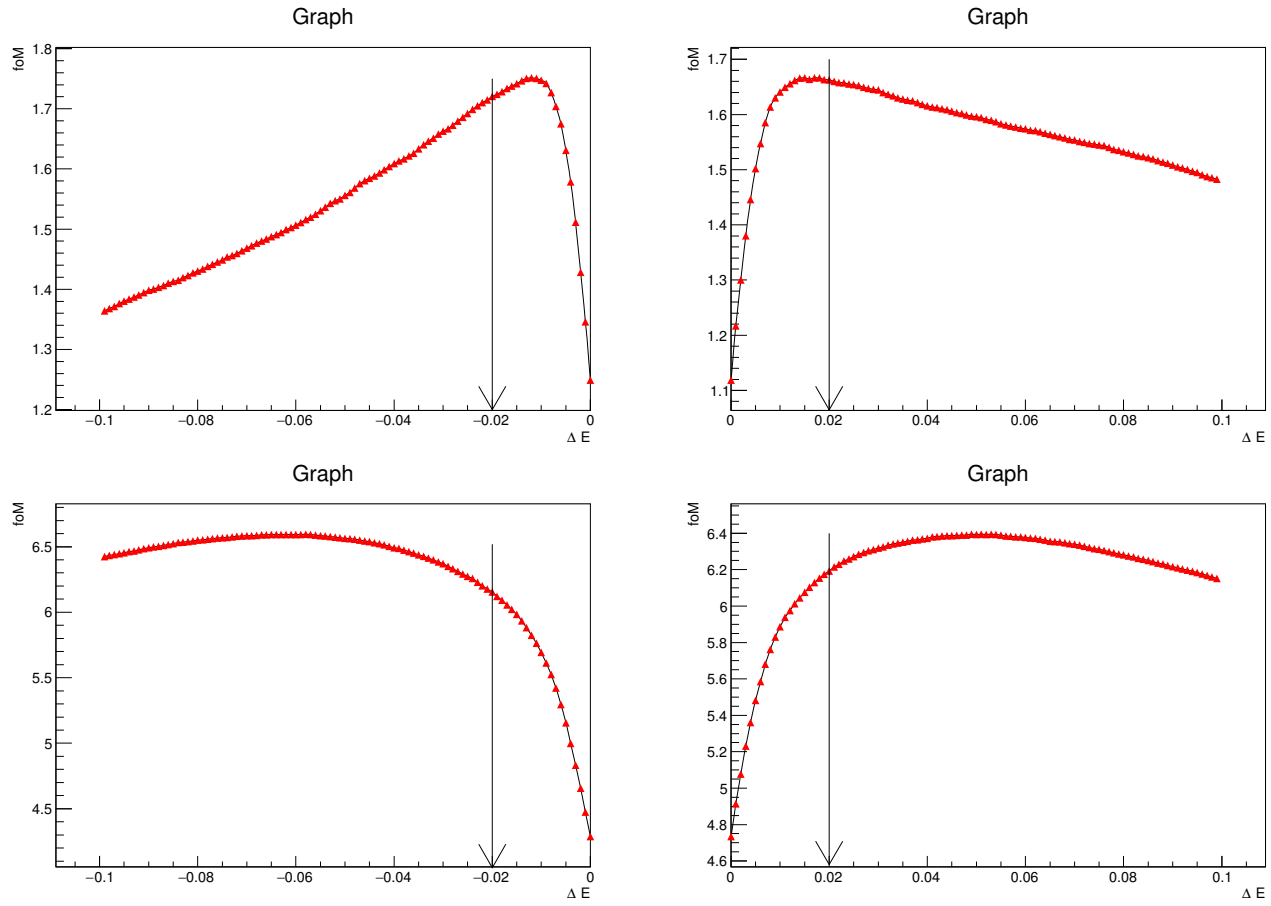

Figure 3.8: Figure of merit for $\Delta E < 0$ (left) and $\Delta E > 0$ (right). $X(3872)$ (top) and $X(3915)$ (bottom)

the figure of merit (FoM) value to be maximum.

$$FoM = \frac{N_{sig}}{\sqrt{N_{sig} + N_{bkg}}} \tag{3.8}$$

N_{sig} is the yield of reconstructed signal events from MC and N_{bkg} represents that of background estimated from $B \to J/\psi X$ inclusive MC sample.

$$N_{sig} = \frac{\text{number of signal events}}{\text{1 million}} \times \mathcal{B}.\mathcal{F} \times 771.6 \times 10^6$$

$$\mathcal{B}.\mathcal{F} \equiv \mathcal{B}.\mathcal{F}(B^{\pm} \to XK^{\pm}) \times \mathcal{B}.\mathcal{F}(X \to J/\psi\omega) \times \mathcal{B}.\mathcal{F}(J/\psi \to \ell^{\pm}) \times \mathcal{B}.\mathcal{F}(\omega \to \pi^{\pm}) \times \mathcal{B}.\mathcal{F}(\pi^0 \to \gamma\gamma) \tag{3.9}$$

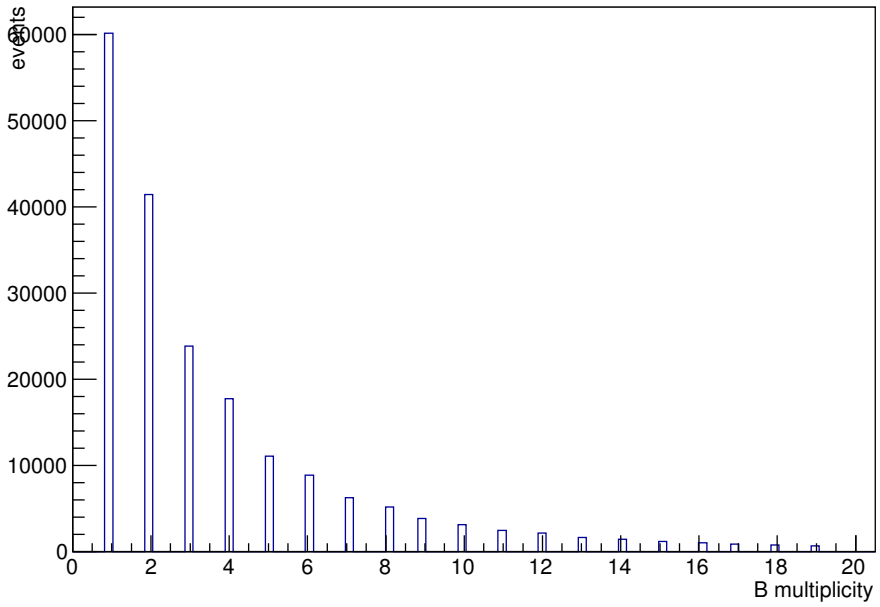

Figure 3.9: Multiplicity of reconstructed B

Signal events will have a ΔE value close to zero. Therefore lower bound of the ΔE selection window should be a negative value and the upper bound a positive.
To find the lower bound, an arbitrary positive value has chosen and a negative value varying from -0.2 to 0 GeV should be taken. The events which fall in these intervals (windows) were considered and the FoM values were calculated for each intervals. Then FoM versus negative ΔE value graph was plotted and the ΔE with maximum FoM value was taken as lower bound.
Similar process has done with to obtain the upper bound of ΔE window, by fixing the lower bound
The ΔE region obtained through this method is -0.02 $<$ ΔE $<$ 0.02 GeV/c^2.

Best candidate selection (BCS)

Even though the above cuts are applied, still multiple B candidates survive after the reconstruction. In order to select the best candidate among them, two methods were tested,

- M_{bc} closest to the nominal B mass value.
  Among the multiple B meson candidates, the one with M_{bc} value closest to the PDG[16] value of B mass is selected.

- χ^2 fitting

$$\chi^2 = \chi^2_V + (\frac{M_{\ell\ell} - m_{J/\psi}}{\sigma_{J/\psi}})^2 + (\frac{M_{\pi^+\pi^-\pi^0} - m_\omega}{\sigma_\omega})^2 + (\frac{M_{\gamma\gamma} - m_{\pi^0}}{\sigma_{\pi^0}})^2 + (\frac{M_{\rm bc} - 5.279}{\sigma_{M_{\rm bc}}})^2 \quad (3.10)$$

M is the reconstructed mass and m is the PDG mass value. σ is the mass width. χ^2_V is obtained by vertex fitting of all the charged tracks. Similarly χ^2 values for $M_{\rm bc}$, masses of J/ψ, ω, π^0 are obtained and summed and the candidate with least value is selected.

$M_{\rm bc}$ is plotted and counted the true events that can be reconstructed if each of the above mentioned B candidate selection is used.

	Total true events	Selected true events	Efficiency of BCS
$M_{\rm bc}$ based BCS	46414	20683	45%
χ^2 based BCS	46414	29996	65%

Table 3.1: Signal efficiency calculated from Monte Carlo study.

From the Table 3.1 it is evident that χ^2 selection method is more efficient in selecting the true events out of the total available true candidates in case of multiple reconstructed B events. The BCS efficiency by χ^2 selection method is 44% more efficient than the $M_{\rm bc}$ selection method.

3.5 Background study

3.5.1 Inclusive MC

To study the possible sources of the background, $B \to J/\psi X$ inclusive MC samples are analyzed. This MC includes all the known B decay modes where the final states contain at least one J/ψ candidate. It is expected that non-J/ψ background to be negligible. This inclusive MC sample corresponds to 100 times the data used in this analysis.

$B \to J/\psi X$ sample is processed through analysis code and different sources of the background are tagged. Since we are interested in $X(3872) \to J/\psi\omega$ the invariant mass, $M_{J/\psi\omega}$ is checked.

In Figure 3.10 (left), $M_{J/\psi\omega}$ of signal along with peaking backgrounds are clearly

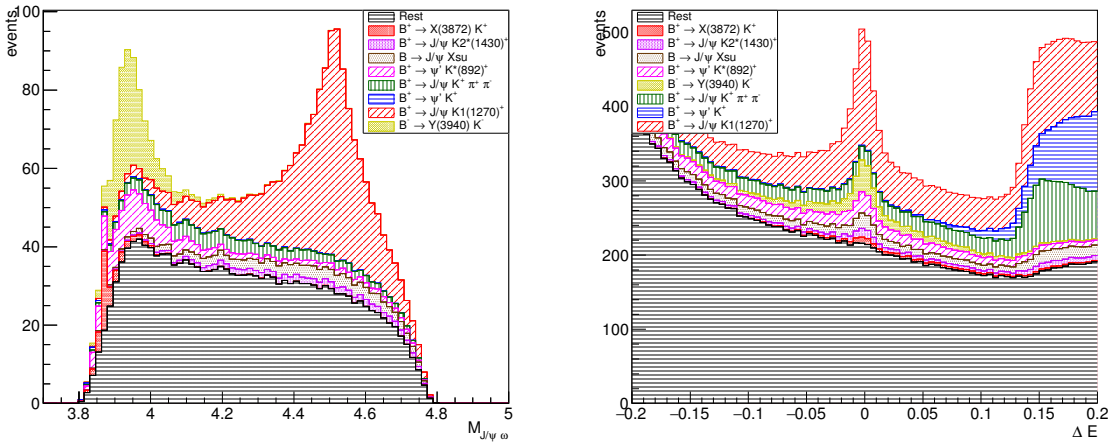

Figure 3.10: Major peaking background

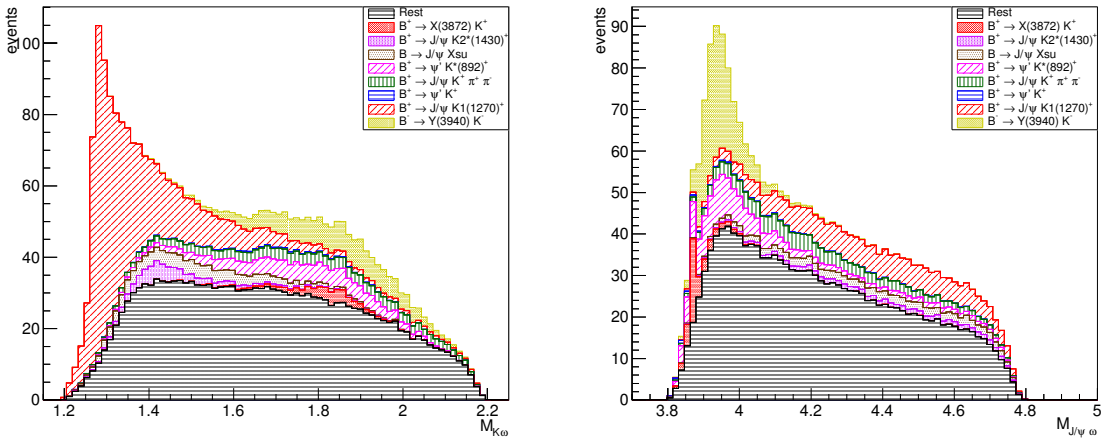

Figure 3.11: Major peaking backgrounds along with signals. $Y(3940)$ mentioned here is actually $X(3915)$.

shown and are tagged. To reduce those unwanted peaks other parameters are also studied.

In Figure 3.10 (right), the ΔE for all modes in inclusive MC is plotted. As explained, -0.02 GeV $< \Delta E <$ 0.02 GeV cut is used for signal identification and one can clearly see that in this region also peaking background survives.

From Figure 3.11 (left), one can clearly see that the most of the $B \to J/\psi K1(1270)^+$ decay events can be removed by applying a cut of $M_{K\omega} > 1.4$ GeV/c^2 while plotting $M_{J/\psi\omega}$. After applying the cut $M_{J/\psi\omega}$ plot got modified as shown in Figure 3.11 (right).

3.6 Signal extraction

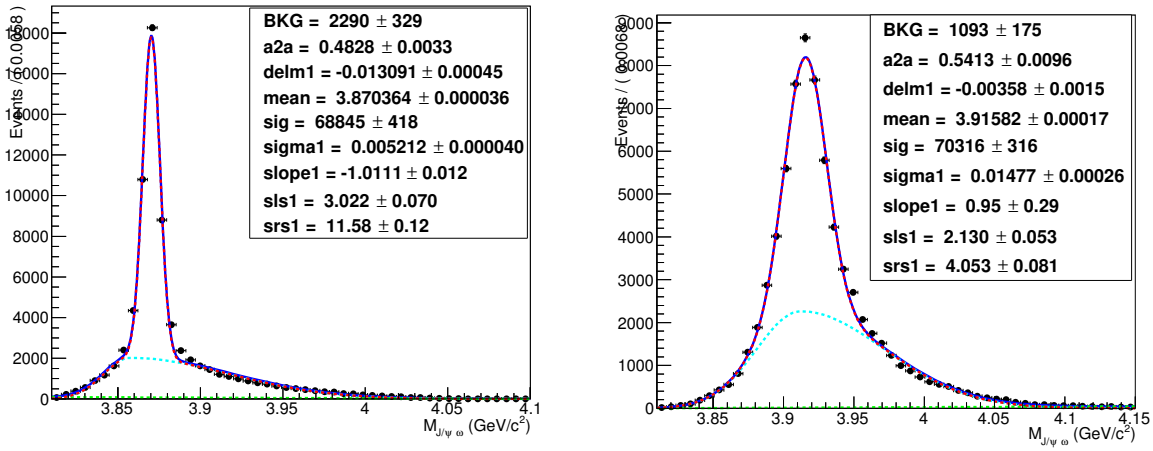

Figure 3.12: UML fit for $M_{J/\psi\omega}$ (left) for $X(3872)$ and $X(3915)$ (right)

Unbinned maximum likelihood (UML) fit is performed to the reconstructed invariant mass, $M_{J/\psi\omega}$, in order to extract the signal yield.
Likelihood for $B \to XK$ can be written as

$$\mathcal{L} = \frac{e^{-N}}{N!}\prod_{i=1}^{N}\{bkg \times Polynomial(M_{J/\psi\omega}; slope1) + sig\times(Gaussian+Bifurcated\,Gaussian)(M_{J/\psi\omega}; mean, sig, delm1, a2a, sls1, srs1)\} \tag{3.11}$$

Figure 3.12 shows the UML fit to the $B \to X(3872)K$ and $B \to X(3915)K$ signal MC. Signal efficiency is observed as 6.88% and 7.03% respectively based on one million generated events. From this one can estimate the expected number of signal events in real data as:

$$\text{Expected events} = \text{efficiency} \times \mathcal{B}.\mathcal{F} \times 771.6 \times 10^6$$
$$\mathcal{B}.\mathcal{F} \equiv \mathcal{B}.\mathcal{F}(B^{\pm} \to XK^{\pm})\times\mathcal{B}.\mathcal{F}(X \to J/\psi\omega)\times\mathcal{B}.\mathcal{F}(J/\psi \to \ell^{\pm})\times\mathcal{B}.\mathcal{F}(\omega \to \pi^{\pm})\times\mathcal{B}.\mathcal{F}(\pi^0 \to \gamma\gamma) \tag{3.12}$$

Around 35 signal events for $X(3872)$ and 170 signals for $X(3915)$ are expected.

Figure 3.13 shows the fit to $B \to J/\psi X$ inclusive MS sample (100 times the data).

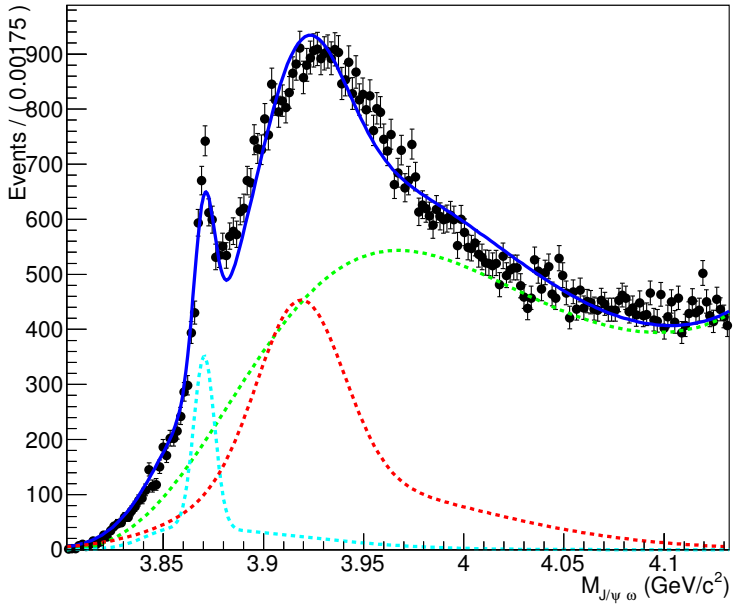

Figure 3.13: Blue curve: UML fit to the $M_{J/\psi\omega}$ distribution of $B \to J/\psi X$ inclusive MC sample (100 times data) to extract $B \to X(3872)K$ and $B \to X(3915)K$. Cyan curve: Fit PDF of $B \to X(3872)K$. Red curve: Fit PDF of $B \to X(3915)K$. Green curve: Threshold function.

One expect to have similar kind of fit in data. Likelihood for the total fit is

$$\mathcal{L} = \frac{e^{-N}}{N!}\prod_{i=1}^{N}\{bkg \times Threshold$$

$$+sig1\times(Gaussian+Bifurcated\,Gaussian)+sig2\times(Gaussian+Bifurcated\,Gaussian)\} \tag{3.13}$$

Here the threshold function is defined as

$$(M - M_{Th})^2 \exp(a(M - M_{Th}) + b(M - M_{Th})^2 + c(M - M_{Th})^3) \tag{3.14}$$

Still, there is scope for fine tuning the fit (which is beyond the scope of this thesis) and will be attempted as next step.

Chapter 4

Results and conclusions

Reconstruction code to analyze the $B \to (J/\psi\omega)K$ decay mode was prepared. MC samples have been generated. Using these samples, signal optimization has done.

In case of multiple candidates, we select the best candidate using least χ^2 method. The method is 44% more efficient as compared to $M_{\rm bc}$ based BCS.

All the possible background modes are tagged and understood. $M_{K\omega} > 1.4$ GeV/c^2 cut is used in order to remove the contribution from higher K^*.

Unbinned maximum likelihood fit is performed in order to extract the signal yield. Belle data is found to be sensitive for the measurement of $\mathcal{B}.\mathcal{F}(B \to XK^{\pm})$. We expect 35 signal events for $X(3872)$ and 170 events for $X(3915)$ on the basis of our signal efficiency.

Appendix A

Decay files for signal generation

A.1 $X(3872)$

```
Alias MyB+ B+
Alias MyB- B-
Alias MyJpsi J/psi
Alias Myomega omega
Alias MyX3872 X(3872)

Decay Upsilon(4S)
0.5    MyB+        B-        VSS;
0.5    B+          MyB-      VSS;
Enddecay

Decay MyB+
1.0    MyX3872     K+        PHOTOS   PHSP;
Enddecay

Decay MyB-
1.0    MyX3872     K-        PHOTOS   PHSP;
Enddecay

Decay MyX3872
```

```
1.0     MyJpsi      Myomega PHOTOS   PHSP;
Enddecay

Decay MyJpsi
0.0593   e+         e-         PHOTOS   VLL;
0.0588   mu+        mu-        PHOTOS   VLL;
Enddecay

Decay Myomega
0.89401  pi-        pi+        pi0      PHOTOS   OMEGA_DALITZ;
Enddecay

End
```

A.2 $X(3915)$

```
Alias MyB+ B+
Alias MyB- B-
Alias MyJpsi J/psi
Alias Myomega omega
Alias MyY3940 X(3915)

Decay Upsilon(4S)
0.5     MyB+        B-         VSS;
0.5     B+          MyB-       VSS;
Enddecay

Decay MyB+
1.0     MyY3940     K+         PHOTOS   PHSP;
Enddecay

Decay MyB-
1.0     MyY3940     K-         PHOTOS   PHSP;
```

```
Enddecay

Decay MyY3940
1.0     MyJpsi      Myomega PHOTOS   PHSP;
Enddecay

Decay MyJpsi
0.0593   e+         e-         PHOTOS   VLL;
0.0588   mu+        mu-        PHOTOS   VLL;
Enddecay

Decay Myomega
0.89401  pi-        pi+        pi0        PHOTOS   OMEGA_DALITZ;
Enddecay

End
```

Bibliography

[1] T. Barnes, S. Godfrey, and E. S. Swanson, Physical Review D. **72**, 054023 (2005).

[2] E. Prencipe, arXiv:1411.0720 (2014).

[3] S. K. Choi, *et al.* Physical review letters **91**, 262001 (2003).

[4] P. del Amo Sanchez, *et al.* Physical Review D. **82**, 011101 (2010).

[5] S. Olsen, *et al.* AIP Conference Proceedings **1701**, 050017 (2016).

[6] A. Hosaka, *et al.* Progress of Theoretical and Experimental Physics **2016**, 062C01 (2016).

[7] L. Maiani, *et al.* Physical Review D. **71**, 014028 (2005).

[8] S. K. Choi. arXiv:1101.5691 (2011).

[9] K. Terasaki, arXiv:1411.7483 (2014).

[10] A. J. Bevan, *et al.* (Belle and BaBar collaboration) The European Physical Journal C, **74**, 1–928 (2014).

[11] S. Kurokawa, and E. Kikutani, Nuclear Instruments and Methods in Phys. Res. A **499**,1-7 (2003).

[12] A. Abashian, *et al.*, Nuclear Instruments and Methods in Phys. Res. A **479**,117-232 (2002).

[13] D. J. Lange, Nucl. Instrum. Methods Phys. Res. A **462**,152 (2001).

[14] R. Brun *et al.*, GEANT3.21, CERN Report No. DD/EE/84-1, 1984.

[15] G. C. Fox and S. Wolfram, Phys. Rev. Lett. **41**, 1581 (1978)

[16] C. Patrignani et al.(Particle Data Group), Chin. Phys. C. **40**, 100001 (2016).